Scientific Research Publishing

Materials Sciences and Applications, 2021, 12, 622-638
https://www.scirp.org/journal/msa
ISSN Online: 2153-1188
ISSN Print: 2153-117X

Optical Properties of Iron to 30 eV

Jerome K. Butler[1], Maria Martinez[2*], Reyhane Kilci[1], Gary A. Evans[1]

[1]Southern Methodist University, Dallas, USA
[2]Federal Center for Technological Education Celso Suckow da Fonseca, CEFET/RJ, Avenida Maracanã, Rio de Janeiro, Brazil
Email: *maria.martinez@cefet-rj.br

How to cite this paper: Butler, J.K., Martinez, M., Kilci, R. and Evans, G.A. (2021) Optical Properties of Iron to 30 eV. *Materials Sciences and Applications*, **12**, 622-638.
https://doi.org/10.4236/msa.2021.1212042

Received: November 30, 2021
Accepted: December 28, 2021
Published: December 31, 2021

Abstract

A modified approach closely related to the Drude, Lorentz-Drude and Brendel-Bormann theories is developed to fit the experimental data of the optical properties of metals. This work, while simplifying and redefining the parameters of previous models, can be directly compared with the parameters of the Brendel-Bormann model. As a test of validity, our model is compared with the Brendel-Bormann model and experimental data for gold. Our model shows excellent agreement with the experimental data for gold (up to 5 eV) and iron (up to 30 eV).

Keywords

Isolators, Waveguides, Optical Properties, Metals

1. Introduction

This work is motivated by the need for the optical characteristics of ferromagnetic materials, especially iron, for use in waveguide optical isolators. These metals may be used as one or more layers of an optical waveguide or they may be used as metal "dopant" atoms or clusters of metal atoms in a host material such as a semiconductor, glass or polymer to form one or more ferromagnetic layers in an optical waveguide [1] [2] [3] [4] [5]. Ferromagnetic materials are anisotropic and are characterized by a susceptibility tensor with non-zero off-diagonal elements whose values change with an applied magnetic field. Designing waveguide isolators requires accurate knowledge of such susceptibility tensors which are obtained from the electronic band structure of materials [6]-[11].

Ehrenheich *et al.* [6] analyzed experimental data for the dielectric constants for silver and copper from 1 to 25 eV with the help of three mechanisms which are free electron effects, interband transitions, and plasma oscillations. In order to distinguish plasma transitions from interband transitions, theoretical values

of the real $\Re\{\varepsilon\}$ and imaginary parts $\Im\{\varepsilon\}$ of the dielectric constant, as well as the loss function $\Im\{\varepsilon^{-1}\}$ were plotted as a function of photon energy. They acquire average optical mass values for silver and copper for the free electron effect region by combining the theoretical and experimental values of the dielectric constant. In 1987, Adachi used a harmonic oscillator model with a critical point-parabolic band model that incorporated Lorentzian broadening and temperature dependence to find optical constants as a function of alloy composition for Zinc-Blende semiconductors [7]. The resulting model showed that contributions from indirect transitions can be significant [7].

The Drude model for the permittivity (based on free electrons) [12] [13] [14] was extensively used until the late 1980s to obtain the optical constants of metals. An extension of this model, referred to as the Lorentz-Drude (LD) model included bound electrons by assuming damped harmonic oscillators at critical wavelengths that correspond to interband transitions [15] [16] [17] [18].

Brendel and Bormann (BB) extended previous work to obtain optical constants of amorphous solids in the infrared by including a superposition of oscillators at critical wavelengths with linewidths that were a convolution of Gaussian and Lorentzian linewidths (Voigt profiles) [10], resulting in good agreement with experimental values at room temperatures [11]. Rakic *et al.* applied the BB approach to obtain optical constants for various metals in the infrared, visible and ultraviolet regions [17].

In this work, we build on the BB model and the work of Rakics' to obtain a model for the optical constants of iron based on experimental data [19] [20]. We verify our model by comparing our theoretical calculations to the experimental data for gold and to Rakics' theoretical model for gold. Our modified BB model used a reduced number of parameters yet provides excellent agreement with experimental data.

2. Optical Properties of Iron

To evaluate the susceptibility of iron under the influence of an external magnetic bias it is necessary to model the valence electrons that play a major role in the characteristics of metals. The Drude model assumed that free electrons determined the susceptibility while the LD model included valence and other bound electrons in the susceptibility calculation [21].

The optical properties of iron have been extensively studied experimentally with results that are somewhat divergent. However, several data indicate similar interband transitions of bound electrons that produce undulations in the susceptibility as a function of photon energy.

The susceptibility in **Figure 1** was calculated from the refractive index and extinction coefficients [19] [20] [22], obtained from optical reflection of light from films. The divergence of the results is probably due to oxide formations on the surface [22] which tends to reduce the reflections and thus lower the value of the dielectric constants. Note that the spurious data for χ_{r}^{b} and χ_{i}^{b} at $h\nu \approx 5.5$ eV

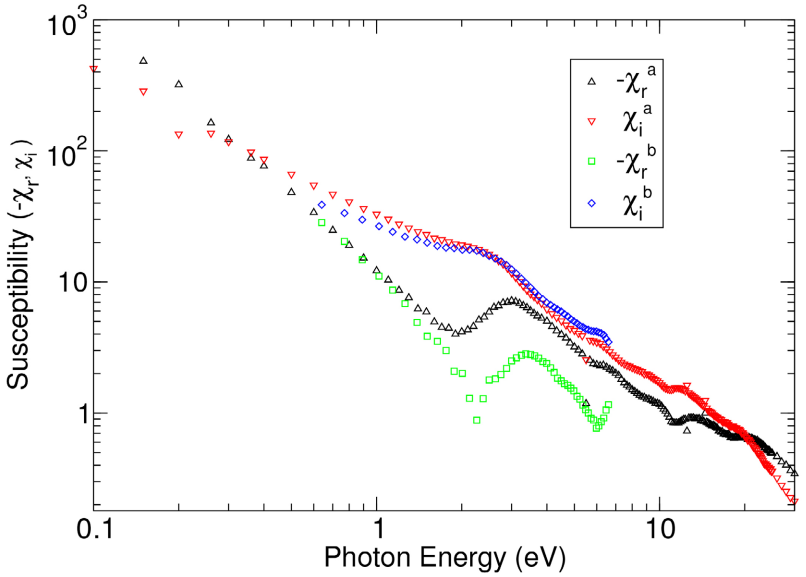

Figure 1. The real, χ_r, and imaginary, χ_i, parts of the susceptibility of iron as a function of photon energy. Data for χ_r^a and χ_i^a is computed from references [19] [20] while data for χ_r^b and χ_i^b is computed from reference [22].

does not appear in the data for χ_r^a and χ_i^a while the spurious data in χ_r^a and χ_i^a at $h\nu \approx 2.25$ eV does not appear in the data for χ_r^b and χ_i^b.

2.1. Electron Displacement in an Electromagnetic Field

The dielectric constant of metals such as nanoparticles composed of iron, cobalt, or nickel can be developed assuming some of the electrons from each atomic site are free to move about within the metal while some are bound to the nucleus at each atomic site. Furthermore, it is generally assumed that only valence electrons participate in the behavior of the dielectric constant. Drude's theory assumed that the free electrons in metals [23] [24] explained the behavior of the dielectric constant or conductivity at low frequencies (below microwave frequencies). For example, the DC conductivity of metals is determined from the slope of the imaginary part of the susceptibility χ_i at low energy photons. At higher photon energies ($E = h\nu > 0.1$ eV) the electrons bound to atomic sites greatly influence the behavior of the susceptibility and produce the undulations in the real and imaginary parts of the susceptibility such as that illustrated in **Figure 1**. Note that both sets of data for iron show a type of resonance at about 2.5 eV.

The force produced by an electromagnetic field acting on a (free or bound) electron of charge q and velocity $\mathbf{v}$ is given by the Lorentz force

$$\mathbf{F} = q\left[\mathbf{e}(t) + \mathbf{v}\times\left(\mathbf{b}(t) + \mathbf{B}_s\right)\right] \approx q\left[\mathbf{e}(t) + \mathbf{v}\times\mathbf{B}_s\right], \tag{1}$$

where $\mathbf{e}$ and $\mathbf{b}$ are a wave's time varying electric and magnetic fields while $\mathbf{B}_s = \hat{\mathbf{x}}B_1 + \hat{\mathbf{y}}B_2 + \hat{\mathbf{z}}B_3$ is an externally-applied static magnetic field. In (1) the force due to a wave's magnetic field, $\mathbf{b}(t)$, may be neglected compared to force produced by the wave's electric field, $\mathbf{e}(t)$. For example, a plane wave has the

ratio $|\mathbf{b}|/|\mathbf{e}| = n/c$, where n is the refractive index. Since the velocity of electrons is much smaller than c, (1) is a good approximation of the force acting on a free electron.

The Drude model assumes an unbound electron has an equation of motion that can be written as

$$m^*\left(\frac{\partial^2\mathbf{r}}{\partial t^2}+\gamma_c\frac{\partial\mathbf{r}}{\partial t}\right)=\mathbf{F} \tag{2}$$

where $\mathbf{r}$ is the electron position relative to an atom, m^* is the electron effective mass, γ_c is a "damping factor" related to electron collisions with atomic sites.

Lorentz modified Drude's theory by assuming electrons bound to the nucleus have a harmonic-like restoring force so that (2) was modified to include the restoring force $k\mathbf{r}$. There are numerous electrons bound to the nucleus and each exhibits different resonant and collision frequencies. Quantum mechanically, an electron may occupy different discrete energy levels that are separated according to the solution of the Schrodinger equation for the harmonic oscillator and the electron may move from one level to another and the electron lifetime at a certain energy level is inversely related to the "damping constant", γ_i [25].

The modified equation of motion of, say, the i^{th} electron is

$$m_i^*\left(\frac{\partial^2\mathbf{r}_i}{\partial t^2}+\gamma_i\frac{\partial\mathbf{r}}{\partial t}+\omega_i^2\mathbf{r}_i\right)=\mathbf{F} \tag{3}$$

where the resonant frequency of the harmonic oscillator is $\omega_i=\left(k_i/m_i^*\right)^{1/2}$. Equation (3) has been frequently used to model dispersion in dielectrics, conductors, and plasmas [21] [25] [26] [27]. (The equation of motion for an electron in the Drude model can be obtained from (3) by placing $\omega_1=0$, *i.e.*, $i=1$ denotes free electrons).

For a harmonic time variation $\exp j\omega t$ of the electromagnetic field, the displacement vector $\mathbf{r}_i=\mathbf{R}_i\exp j\omega t$, $\mathbf{v}_i=j\omega\mathbf{R}_i\exp j\omega t$, $\mathbf{e}(t)=\mathbf{E}\exp j\omega t$ and $\mathbf{b}(t)=\mathbf{B}\exp j\omega t$, so that (3) can be written as

$$\left(\omega_i^2+j\omega\gamma_i-\omega^2\right)\mathbf{R}_i=\frac{q}{m^*}\left(\mathbf{E}+j\omega\mathbf{R}_i\times\mathbf{B}_s\right). \tag{4}$$

The vector product may be written as

$$\mathbf{R}_i\times\mathbf{B}_s=\ddot{\mathrm{B}}_s\cdot\mathbf{R}_i,$$

where $\ddot{\mathrm{B}}_s$ is the asymmetric dyad (in matrix form)

$$\ddot{\mathrm{B}}_s=\begin{pmatrix}0 & B_z & -B_y\\ -B_z & 0 & B_x\\ B_y & -B_x & 0\end{pmatrix}. \tag{5}$$

For free and bound electrons (4) may be written as

$$\left(\ddot{\mathrm{I}}-\ddot{\mathrm{B}}_i\right)\cdot\mathbf{R}_i=\frac{1}{j\omega\tilde{\Lambda}_i}\mathbf{E}, \tag{6}$$

where $\tilde{\Lambda}_i = j\omega m^* \tilde{\Omega}_i / q$, $\tilde{\Omega}_i = 1 - \Omega_i^2 - j\Gamma_i$, $\Omega_i = \omega_i / \omega$ is the normalized resonant frequency, $\Gamma_i = \gamma_i / \omega$ is the normalized collision frequency, $\vec{\mathrm{I}}$ is the unit dyad and the frequency-dependent dyad $\vec{\mathrm{B}}_i(\omega)$ is

$$\vec{\mathrm{B}}_i(\omega) = \begin{pmatrix} 0 & b_{zi}(\omega) & -b_{yi}(\omega) \\ -b_{zi}(\omega) & 0 & b_{xi}(\omega) \\ b_{yi}(\omega) & -b_{xi}(\omega) & 0 \end{pmatrix}, \tag{7}$$

where $b_{xi}(\omega) = B_x / \tilde{\Lambda}_i(\omega)$. The components $b_{yi}(\omega)$ and $b_{zi}(\omega)$ satisfy similar expressions (Note that $\tilde{\Lambda}_i$ has the dimension of the magnetic field, which is Tesla in SI units). In the absence of a static magnetic field, $\vec{\mathrm{B}}_i = \vec{0}$, the zero dyad.

The solution for the electron displacement from the nucleus is

$$\mathbf{R}_i = \frac{1}{j\omega\tilde{\Lambda}_i}\left(\vec{\mathrm{I}} - \vec{\mathrm{B}}_i(\omega)\right)^{-1} \cdot \mathbf{E}, \tag{8}$$

and the inverse is

$$\left(\vec{\mathrm{I}} - \vec{\mathrm{B}}_i(\omega)\right)^{-1} = \frac{1}{1 + \left(B_s / \tilde{\Lambda}_i\right)^2} \begin{pmatrix} 1 + b_{xi}^2 & b_{xi}b_{yi} + b_{zi} & b_{xi}b_{zi} - b_{yi} \\ b_{xi}b_{yi} - b_{zi} & 1 + b_{yi}^2 & b_{yi}b_{zi} + b_{xi} \\ b_{xi}b_{zi} + b_{yi} & b_{yi}b_{zi} - b_{xi} & 1 + b_{zi}^2 \end{pmatrix}, \tag{9}$$

where $B_s^2 = B_x^2 + B_y^2 + B_z^2$. When the static field is directed along *x*, *y*, or *z*, there is only one off-diagonal component of $\left(\vec{\mathrm{I}} - \vec{\mathrm{B}}_i\right)^{-1}$. For the case of a static field directed along the *y* axis, $\mathbf{B}_s = \hat{\mathbf{y}} B_s$,

$$\left(\vec{\mathrm{I}} - \vec{\mathrm{B}}_i(\omega)\right)^{-1} \approx \begin{pmatrix} 1 & 0 & B_s / \tilde{\Lambda}_i \\ 0 & 1 & 0 \\ B_s / \tilde{\Lambda}_i & 0 & 1 \end{pmatrix}. \tag{10}$$

The resulting dipole moment is $\mathbf{p}_i = q\mathbf{R}_i$ has a single off-axis component.

2.2. Electric Susceptibility from the Lorentz-Drude Model

When the dipole moment for a single charge is $\mathbf{p}_1 = q\mathbf{R}_1$, the polarization produced by the free charges becomes

$$\mathbf{P}_1 = N_1 \mathbf{p}_1 = \varepsilon_o \vec{\mathrm{X}}_1 \cdot \mathbf{E}, \tag{11}$$

where N_1 is the number of electrons per unit volume that have the dipole moment $\mathbf{p}_1$. The Drude model for most metals does not generally fit to the computed values of susceptibility determined from experimental measurements used to estimate the index of refraction and extinction coefficients in the infrared. However, it does give a reasonable representation at DC to microwave frequencies.

When the static magnetic field is directed along *y*, there are 2 off-diagonal components of the susceptibility so the susceptibility dyadic can be written as

$$\vec{\mathrm{X}} = \begin{pmatrix} \chi_v & 0 & \chi_o \\ 0 & \chi_c & 0 \\ -\chi_o & 0 & \chi_v \end{pmatrix}. \tag{12}$$

Defining the plasma frequency as $\omega_{p1}^2 = q^2 N_1 / \varepsilon_o m_1^*$, and a complex norma-

lized frequency for "free electrons" as $\tilde{\Omega}_1 = 1 - j\Gamma_1$, and a normalized collision frequency as $\Gamma_1 = \gamma_1/\omega$, so that the electric susceptibility due to free electrons becomes

$$\ddot{\mathrm{X}}_1 = \frac{N_1 q}{j\varepsilon_o \omega \tilde{\Lambda}_1}\left(\ddot{\mathrm{I}} - \ddot{\mathrm{B}}_1\right)^{-1} = -\frac{\Omega_{p1}^2}{\tilde{\Omega}_1}\left(\ddot{\mathrm{I}} - \ddot{\mathrm{B}}_1\right)^{-1}. \tag{13}$$

In the absence of a static magnetic field, the dyad $\ddot{\mathrm{B}}_1 = \ddot{0}$ so the susceptibility is a scalar times the unit dyad, where the scalar value is

$$\chi_1 = -\frac{\Omega_{p1}^2}{\tilde{\Omega}_1} = -\frac{\omega_{p1}^2}{\omega^2 + \gamma_1^2} - j\frac{\omega_{p1}^2 \gamma_1}{\omega\left(\omega^2 + \gamma_1^2\right)} \tag{14}$$

and thus χ_1 is the susceptibility due to the free electrons. Because the harmonic time variation is of the form $\exp(j\omega t)$, the real and imaginary parts of χ_1 are negative and its imaginary part has a singularity at $\omega = 0$, implying the low frequency conductance is $\sigma = \varepsilon_o \omega_{p1}^2/\gamma_1$. The diagonal component is $\chi_c = \chi_1$, the susceptibility in the absence of a magnetic bias, while the "variable" part

$$\chi_v = \frac{\chi_c}{1 + \left(B_s/\tilde{\Lambda}_1\right)^2} \approx \chi_c. \tag{15}$$

The off-diagonal component satisfies

$$\chi_o = \frac{\Omega_{p1}^2}{\tilde{\Omega}_1}\frac{B_s/\tilde{\Lambda}_1}{1 + \left(B_s/\tilde{\Lambda}_1\right)^2} \approx j\Omega_{p1}^2 \mathcal{M}_1^* \Omega_{cy}\frac{1}{\tilde{\Omega}_1^2}, \tag{16}$$

where Ω_{cy} is the normalized cyclotron frequency, and using $q = -e$, $\Omega_{cy} = eB_s/m_e/\omega$, and $\mathcal{M}_1^* = m_e/m_1^*$ is the ratio of the mass of the electron and effective mass of the free electron. With a static field of 1 Tesla, the cyclotron frequency $\omega_{cy} \approx 0.116$ meV is just a measure of the static field strength. The diagonal components of the susceptibility dyad contain the electron effective mass in the expression of the plasma frequency. However, the off-diagonal elements depend explicitly on the effective mass. The relative anisotropic dielectric constant is obtained from (12) and the unit dyad.

There are only two parameters in the Drude model of the electric susceptibility, ω_{p1} and γ_1 and they may be estimated from experimental data [14]. Here it is estimated that for iron $\omega_{p1} \approx 3.5$ eV, while the low-frequency conductivity of iron, $\sigma \approx 1.044 \times 10^7$ Siemens per meter, is used to determine $\gamma_1 = \varepsilon_o \omega_p^2/\sigma \approx 0.0158$ eV (The real part of the susceptibility is rather insensitive to the small values of γ_1, $\Re\{\chi_1\} \approx -\left(\omega_{p1}/\omega\right)^2$, so that it can describe experimental data in the infrared region by adjusting only the plasma frequency for free electrons). **Figure 2** illustrates the result of "fitting" ω_{p1} and γ_1 to the experimental data. In the infrared region, the real part of the susceptibility determined from the Drude model is satisfactory to about 2 eV, however, the imaginary part, $\Im\{\chi_1\}$ diverges from experimental values near 0.1 eV. When $\lambda = 1.55$ μm (≈0.8 eV), the susceptibility of iron is $\chi \approx -19 - j41$ which produces $\left(1 + \chi_1\right)^{1/2} \approx 3.66 - j5.6$ while the Drude model has $\chi_1 \approx -19 - j0.37$ which produces $\left(1 + \chi_1\right)^{1/2} \approx 0.44 - j4.24$.

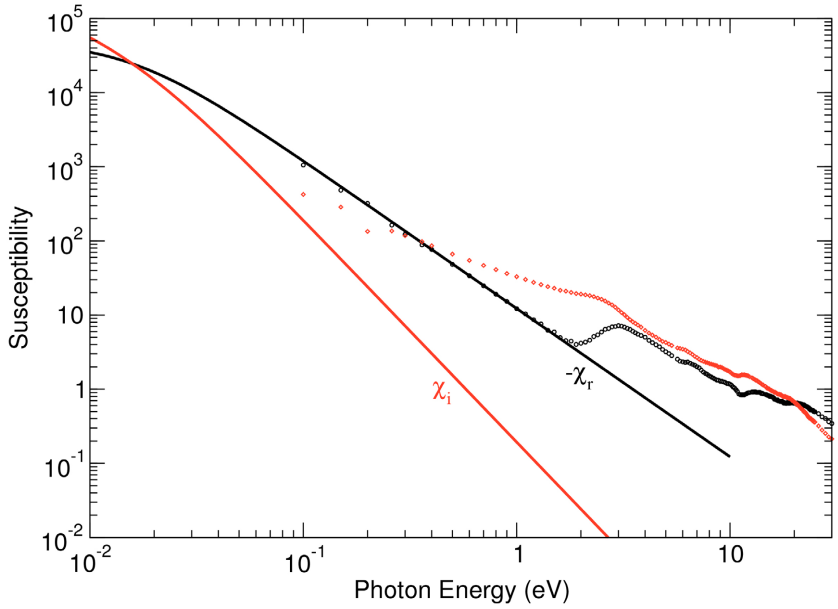

Figure 2. The real, χ_r, and imaginary, χ_i, parts of the susceptibility of iron using the Drude model. The plasma frequency is $\omega_p = 3.5$ eV and the collision frequency is determined from the DC conductivity, σ, $\gamma_1 = \varepsilon_o \omega_p^2 / \sigma$. Experimental values were computed from the data in [19] [20] as in **Figure 1**.

To develop a more comprehensive model of the anisotropic susceptibility of iron the modification of the susceptibility due to the bound electrons of the Lorentz theory are added to the model. Accordingly, the anisotropic susceptibility will be written as

$$\ddot{\mathrm{X}} = \sum_{i=1}^{Z} \ddot{\mathrm{X}}_i, \tag{17}$$

where

$$\ddot{\mathrm{X}}_i = -\frac{\Omega_{\mathrm{p}i}^2}{\tilde{\Omega}_i}\left(\ddot{\mathrm{I}} - \ddot{\mathrm{B}}_i\right)^{-1}, \tag{18}$$

where Z represents the number of electrons that can be bunched into groups having populations N_i electrons per unit volume within each group. As before, N_1 represents free electrons per unit volume while $N_2, N_3, \cdots$ represent the number of bound electrons that can be grouped with identical collision and resonant frequencies. Iron is a transition metal and has about $N_{\mathrm{Fe}} = 8.46 \times 10^{28}$ atoms per cubic meter and 26 electrons per atom so that $N_1 + N_2 + \cdots + N_Z$ cannot exceed $26 N_{\mathrm{Fe}}$.

The off-diagonal component of the susceptibility, $\chi_{13} = \chi_o$, satisfies

$$\chi_o = -\sum_{i=1}^{Z} \chi_i \frac{B_s / \tilde{\Lambda}_i}{1 + \left(B_s / \tilde{\Lambda}_i\right)^2} \approx j\Omega_{\mathrm{cy}} \left(\sum_{i=1}^{Z} \frac{\mathcal{M}_i^* \Omega_{\mathrm{p}i}^{\ 2}}{\tilde{\Omega}_i^2} \right) \tag{19}$$

In the absence of a magnetic bias, the susceptibility tensor is diagonal and that produced by the individual groups, χ_i, of the LD model is given by

$$\chi = \sum_{i=1}^{Z} \chi_i, \tag{20}$$

where

$$\chi_i = -\frac{\Omega_{pi}^{\ 2}}{\tilde{\Omega}_i}. \tag{21}$$

The value χ_1 represents the susceptibility of the free electrons while χ_i, $i = 2, \cdots, Z$ represent the susceptibilities due to various groups of bound electrons, and Z is the number of "bunchable" groups that can be identified by experimental data. The susceptibility tensor may be written in terms of the applied static field and the unbiased group susceptibilities, χ_i as

$$\vec{\vec{\mathrm{X}}} = \sum_{i=1}^{Z} \chi_i \left[\vec{\vec{\mathrm{I}}} - \vec{\vec{\mathrm{B}}}_i(\omega)\right]^{-1}. \tag{22}$$

The electron magnetic dipole moments are determined from a combination of the orbital and spin moments. Because the contribution to the magnetic field from the orbital path of the electron is insignificant compared to that of the electron spin, magnetic moments in iron tend to be dominated by the electron spin [21].

2.3. Susceptibility: Brendel-Bormann Model

The Brendel-Bormann model [10], BB, is a slight extension of the LD theory and was used previously to explain frequency response of the dielectric constant of metals [17]. The resonant frequencies of bound electrons were assumed to be random variables $\bar{\omega}_i$ that have Gaussian distributions centered about ω_i, $i = 2, 3, \cdots, Z$. Thus, the susceptibility given by (22) becomes a random function of the set of random transition frequencies $\{\bar{\omega}_i\}_{i=2}^{Z}$ whose mean values are given by the set $\{\omega_i\}_{i=2}^{Z}$, so that

$$\vec{\vec{\mathrm{X}}}(\omega; \bar{\omega}_2, \bar{\omega}_3, \cdots, \bar{\omega}_Z) = \chi_1(\omega)\left[\vec{\vec{\mathrm{I}}} - \vec{\vec{\mathrm{B}}}_1(\omega)\right]^{-1} \sum_{i=2}^{Z} \chi_i(\omega; \bar{\omega}_i)\left[\vec{\vec{\mathrm{I}}} - \vec{\vec{\mathrm{B}}}_i(\omega)\right]^{-1}. \tag{23}$$

Assuming the random variables are independent, the joint probability density function is assumed to have the Gaussian form

$$\begin{aligned} &p(\bar{\omega}_2, \bar{\omega}_3, \cdots, \bar{\omega}_Z) \\ &= \left[(2\pi)^{(Z-1)/2} \sigma_2 \sigma_3 \cdots \sigma_Z\right]^{-1/2} \mathrm{e}^{-\left[(\bar{\omega}_2-\omega_2)^2/2\sigma_2^2 + (\bar{\omega}_3-\omega_3)^2/2\sigma_3^2 + \cdots + (\bar{\omega}_Z-\omega_Z)^2/2\sigma_Z^2\right]}. \end{aligned} \tag{24}$$

The expected value of the susceptibility tensor becomes

$$\left\langle \vec{\vec{\mathrm{X}}} \right\rangle = \chi_1(\omega)\left[\vec{\vec{\mathrm{I}}} - \vec{\vec{\mathrm{B}}}_1(\omega)\right]^{-1} + \sum_{i=2}^{Z} \left\langle \chi_i(\omega, \bar{\omega}_i)\left[\vec{\vec{\mathrm{I}}} - \vec{\vec{\mathrm{B}}}_i(\omega, \bar{\omega}_i)\right]^{-1} \right\rangle, \tag{25}$$

where

$$\begin{aligned} &\left\langle \chi_i(\omega, \bar{\omega}_i)\left[\vec{\vec{\mathrm{I}}} - \vec{\vec{\mathrm{B}}}_i(\omega, \bar{\omega}_i)\right]^{-1} \right\rangle \\ &= \left(2\pi\sigma_i^2\right)^{-1/2} \int_{-\infty}^{\infty} \chi_i(\omega, \bar{\omega}_i)\left[\vec{\vec{\mathrm{I}}} - \vec{\vec{\mathrm{B}}}_i(\omega, \bar{\omega}_i)\right]^{-1} \mathrm{e}^{-(\bar{\omega}_i-\omega_i)^2/2\sigma_i^2} \mathrm{d}\bar{\omega}_i. \end{aligned} \tag{26}$$

when the static bias is along the y direction,

$$\left\langle \ddot{\mathrm{X}} \right\rangle = \begin{pmatrix} \langle \chi_{\mathrm{v}} \rangle & 0 & \langle \chi_{\mathrm{o}} \rangle \\ 0 & \langle \chi_{\mathrm{c}} \rangle & 0 \\ -\langle \chi_{\mathrm{o}} \rangle & 0 & \langle \chi_{\mathrm{v}} \rangle \end{pmatrix}, \tag{27}$$

where the expected value of χ_{c} is

$$\langle \chi_{\mathrm{c}} \rangle = -\frac{\Omega_{\mathrm{p1}}^{2}}{\tilde{\Omega}_{1}} - \sum_{i=2}^{Z} \Omega_{\mathrm{p}i}^{2} \left\langle \frac{1}{\tilde{\Omega}_{i}} \right\rangle, \tag{28}$$

which is independent of bias and is thus the susceptibility in the absence of a bias. The expected value of the diagonal component that is dependent on the bias is

$$\langle \chi_{\mathrm{v}} \rangle = -\frac{\Omega_{\mathrm{p1}}^{2}}{\tilde{\Omega}_{1}} \frac{1}{1+\left(B_{\mathrm{s}}/\tilde{\Lambda}_{1}\right)^{2}} - \sum_{i=2}^{Z} \Omega_{\mathrm{p}i}^{2} \left\langle \frac{\tilde{\Omega}_{i}}{\tilde{\Omega}_{i}^{2} - \Omega_{\mathrm{cy}}^{2}} \right\rangle \approx \langle \chi_{\mathrm{c}} \rangle \tag{29}$$

The expected value of the off-diagonal susceptibility tensor is

$$\langle \chi_{\mathrm{o}} \rangle \approx j\Omega_{\mathrm{cy}} \left(\frac{\mathcal{M}_{1}^{*} \Omega_{\mathrm{p1}}^{2}}{\tilde{\Omega}_{1}^{2}} + \sum_{i=2}^{Z} \mathcal{M}_{i}^{*} \Omega_{\mathrm{p}i}^{2} \left\langle \frac{1}{\tilde{\Omega}_{i}^{2}} \right\rangle \right), \tag{30}$$

so that the expected value of χ_{o} depends on $\left\langle 1/\tilde{\Omega}_{1}^{2} \right\rangle$ (see **Appendix**).

3. Formulation, Results and Discussion

The objective here is to match the theoretical susceptibility governed by the LD and the BB theories to the experimental data obtained from unbiased samples of iron. Previous models were concerned with matching the theoretical dielectric constant governed by the LD and the BB theories with experimental data [15] [17]. The approach here somewhat resembles that of Rakic *et al.* [17]. The experimental values in **Figure 1**, given in Weaver *et al.* [19] [20], are used because they are more extensive and extend over a larger range of energies than those given in Johnson and Christy [22]. Some spurious data points were dropped because we were unable to associate neighboring points with the dropped point to produce a so-called resonant transition condition.

In fitting experimental data to theory, the number of variables depends on the number of grouped electrons in the LD model. As discussed earlier, bound electrons have only two unknown parameters: $\omega_{\mathrm{p}i}^{2}$, the square of the plasma frequency, determined from N_i, and the collision frequency γ_i. All bound electrons are collected into different groups according to their plasma, collision and resonant frequencies. Unknown variables are contained in the vector X^{*} and are grouped into sets, namely, the Group 1 set is $\left\{\omega_{\mathrm{p1}}^{2}, \gamma_{1}\right\} = \left\{X_{1}, X_{2}\right\}$, while the Group 2 set is $\left\{\omega_{\mathrm{p2}}^{2}, \gamma_{2}, \omega_{2}\right\} = \left\{X_{3}, X_{4}, X_{5}\right\}$, etc. For free electrons, $\tau_{1} = 1/2\pi\gamma_{1}$ represents the mean time between collisions, while for bound electrons $\tau_{i} = 1/2\pi\gamma_{i}$ is the electron life time at an energy level. The frequency ω_{i} represents the transition frequency when an electron changes from one state to another. Thus, if there are Z groups of electrons, then there will be $N_{Z} = 3Z - 1$ unknown pa-

rameters. The unknowns $X_1, X_3, X_6, \cdots$ are ω_{pi}^2, $i = 1, 3, 6, \cdots$.

The BB model of the dielectric constant is an extension of the LD model [10] [17] and assumes the resonant/transition frequencies exhibit homogeneous/inhomogeneous broadening that can be described by a Gaussian distribution centered at resonant frequencies with a width of σ. The ith oscillator centered at ω_i has a Gaussian width of σ_i and thus adds a new parameter to the X^* vector that must be determined from fitting the theory to the experimental data. Accordingly, Group i data has the parameters $\left\{\omega_{pi}^2, \gamma_i, \omega_i, \sigma_i\right\}$ so that the total number of parameters is $N_Z = 4Z - 2$.

To fit the theoretical susceptibility to experimental data we use a mean-square relative error function given by

$$E\left(X^*\right) = \sum_m W\left(\omega_m\right)\left[E_r^2\left(X^*, \omega_m\right) + E_i^2\left(X^*, \omega_m\right)\right], \tag{31}$$

where the real part is $E_r\left(X^*, \omega_m\right) = \left[\chi_r\left(X^*, \omega_m\right) - \chi_{re}\left(\omega_m\right)\right] \Big/ \chi_{re}\left(\omega_m\right)$. The real part of the theoretical susceptibility at ω_m is $\chi_r\left(X^*, \omega_m\right)$, while $\chi_{re}\left(\omega_m\right)$ is the experimental data at ω_m. The imaginary part, $E_i\left(X^*, \omega_m\right)$ in (31) is obtained by replacing r with i in the above expressions. The weight function $W\left(\omega_m\right) = \left(\omega_{m+1} - \omega_{m-1}\right)/2\omega_m$ is designed so as to represent sparse data equally with bunched data as well as to weigh low energy points equally with high-energy ones. This approach is similar to representing equally spaced data on a log abscissa axis.

The optimization process that minimizes (31) with respect to vector X^* uses the NAG Mark 23 optimization library routine E04LBF [28]. The definition of components of X^* and their relation to the parameters of the BB model of the dielectric constant or susceptibility, defined in (28) are illustrated in **Table 1** and **Table 2**.

Our model is implemented for gold for the sake of comparison with Rakic's work and the data was obtained from Handbook of Optical Constants of Solids [29]. The output of the vector X^* from E04LBF was used to compute the theoretical dielectric of gold. The theoretical calculation of the dielectric constant of gold obtained by Rakic [17] was obtained for comparison to the results obtained by our model. **Figure 3** shows the real and imaginary parts of the dielectric constant as a function of photon energy for both methods.

Table 1 lists the output of appropriate variables from both methods. Furthermore, the implementation of our model for iron data [19] [20] can be seen in Section 4 **Figure 4** shows real and imaginary parts of susceptibility for iron. The computed parameters for the modified BB model of iron are shown in **Table 2**.

Rakics' method used for the analysis of gold employs 6 groups of electrons and incorporates 23 unknowns while our method uses 5 groups of electrons and a total of 18 unknowns. Also, our model uses 1 less unknown for a given group of electrons because the oscillator strength $\omega_{pi}^2 = \omega_p^2 f_i$ is treated as a single variable without the constraint $\sum f_i = 1$.

Table 1. The computed components of the X^* vector that describes the dielectric constant of gold using the BB model results from Ref. [17] (first three columns) and that obtained with the model discussed above. All frequencies, ω_i, damping constants, γ_i, and linewidths, σ_i, have units of eV. Relative oscillator strengths f_is have no units. The term ω_{pi}^2 in this work is equal to $\omega_p^2 f_i$, which are Rakic's parameters.

X_1	ω_p	9.030	X_1	ω_{p1}^2	61.754
X_2	f_1	0.770	X_2	γ_1	0.0521
X_3	γ_1	0.050			
X_4	f_2	0.054	X_3	ω_{p2}^2	4.4306
X_5	γ_2	0.074	X_4	γ_2	0.0643
X_6	ω_2	0.218	X_5	ω_2	0.0100
X_7	σ_2	0.742	X_6	σ_2	0.7954
X_8	f_3	0.050	X_7	ω_{p3}^2	4.7123
X_9	γ_3	0.035	X_8	γ_3	0.0001
X_{10}	ω_3	2.885	X_9	ω_3	2.8913
X_{11}	σ_3	0.349	X_{10}	σ_3	0.3678
X_{12}	f_4	0.312	X_{11}	ω_{p4}^2	35.859
X_{13}	γ_4	0.083	X_{12}	γ_4	0.0001
X_{14}	ω_4	4.069	X_{13}	ω_4	4.2778
X_{15}	σ_4	0.830	X_{14}	σ_4	0.8598
X_{16}	f_5	0.719	X_{15}	ω_{p5}^2	42.881
X_{17}	γ_5	0.125	X_{16}	γ_5	0.0001
X_{18}	ω_5	6.137	X_{17}	ω_5	6.1026
X_{19}	σ_5	1.246	X_{18}	σ_5	0.6107
X_{20}	f_6	1.648	X_{19}	ω_{p6}^2	-
X_{21}	γ_6	0.179	X_{20}	γ_6	-
X_{22}	ω_6	27.970	X_{21}	ω_6	-
X_{23}	σ_6	1.795	X_{22}	σ_6	-

3.1. Dielectric Constant of Gold

The comparative fit of our model with that of Rakic's for the relative dielectric constant of gold is shown in **Figure 3**. Rakic *et al.* pointed out the superiority of the BB model over the LD model [17].

3.2. Susceptibility of Iron

The main aim of this work is to develop a theoretical model for the susceptibility of iron using experimental data. In the original BB paper, the superiority of the Gaussian-Lorentzian convolution over just a Lorentzian profile was explained for amorphous solids in the infrared region [10]. In a similar fashion, Rakic *et al.* showed that the model is applicable for various metals not only for the infrared region, but also for visible and ultraviolet regions. However, Rakic *et al.* did not

work on optical properties of iron. In our work, we apply our model to iron and the computed fit parameters can be seen in Table 2. The main difference between our analysis and Rakics' analysis is the elimination of $\sum f_i = 1$ constraint from the system. In Table 2 the first three columns show Rakic's parameters and the last three columns show the parameters used for this work.

The fit for the susceptibility data of iron in terms of photon energy can be seen in Figure 4. The data is acquired from Weaver *et al.* [19] [20]. The numerical

Table 2. The computed components of the X^* vector describe the susceptibility of iron using modified BB model on experimental data for iron [19]. The first three columns represent the vector X^* as described by Ref. [17] while the last three columns represent the vector X^* obtained with our modified BB model. All frequencies, ω_i, damping constants, γ_i, and linewidths, σ_i, have units of eV. Relative oscillator strengths f_is have no units.

X_1	ω_p	22.46	X_1	ω_{p1}^2	11.50
X_2	f_1	0.0279	X_2	γ_1	0.0084
X_3	γ_1	0.0084			
X_4	f_2	0.3247	X_3	ω_{p2}^2	163.8
X_5	γ_2	5.051	X_4	γ_2	5.051
X_6	ω_2	0.2060	X_5	ω_2	0.2060
X_7	σ_2	0.0000	X_6	σ_2	0.0006
X_8	f_3	0.0387	X_7	ω_{p3}^2	19.50
X_9	γ_3	1.214	X_8	γ_3	1.214
X_{10}	ω_3	2.464	X_9	ω_3	2.464
X_{11}	σ_3	0.3078	X_{10}	σ_3	0.3078
X_{12}	f_4	0.0194	X_{11}	ω_{p4}^2	9.758
X_{13}	γ_4	2.169	X_{12}	γ_4	2.169
X_{14}	ω_4	6.301	X_{13}	ω_4	6.301
X_{15}	σ_4	0.0003	X_{14}	σ_4	0.0003
X_{16}	f_5	0.0121	X_{15}	ω_{p5}^2	6.077
X_{17}	γ_5	0.0000	X_{16}	γ_5	0.0000
X_{18}	ω_5	8.892	X_{17}	ω_5	8.892
X_{19}	σ_5	1.032	X_{18}	σ_5	1.032
X_{20}	f_6	0.0501	X_{19}	ω_{p6}^2	25.25
X_{21}	γ_6	4.014	X_{20}	γ_6	4.014
X_{22}	ω_6	12.25	X_{21}	ω_6	12.25
X_{23}	σ_6	0.0072	X_{22}	σ_6	0.0072
X_{24}	f_7	0.5324	X_{23}	ω_{p7}^2	268.5
X_{25}	γ_7	24.06	X_{24}	γ_7	24.06
X_{26}	ω_7	19.47	X_{25}	ω_7	19.47
X_{27}	σ_7	0.0077	X_{26}	σ_7	0.0077

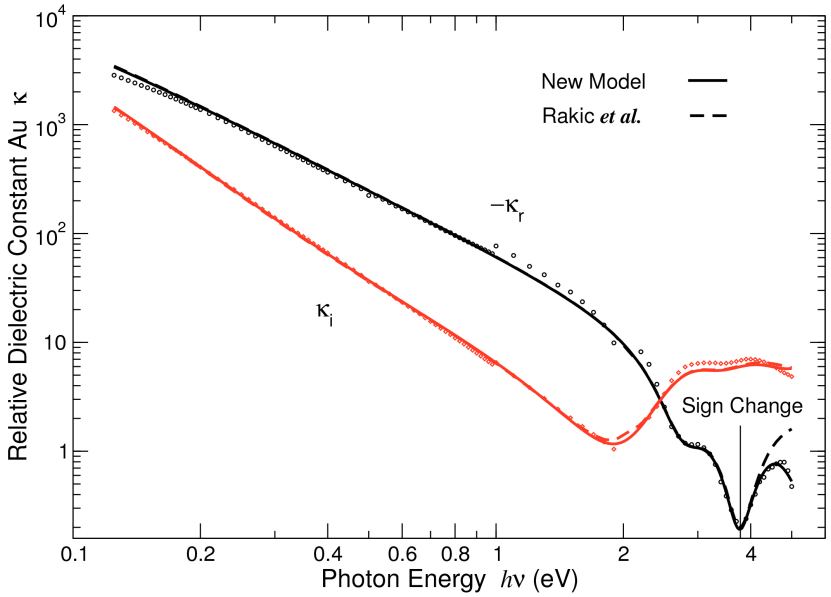

Figure 3. The real, κ_r, and imaginary, κ_i, parts of the dielectric constant of gold using the BB model. Experimental values (small circles) were computed from the data in [29]. The solid curves were obtained by our model while the dashed curves were obtained from the gold data given in Ref. [17].

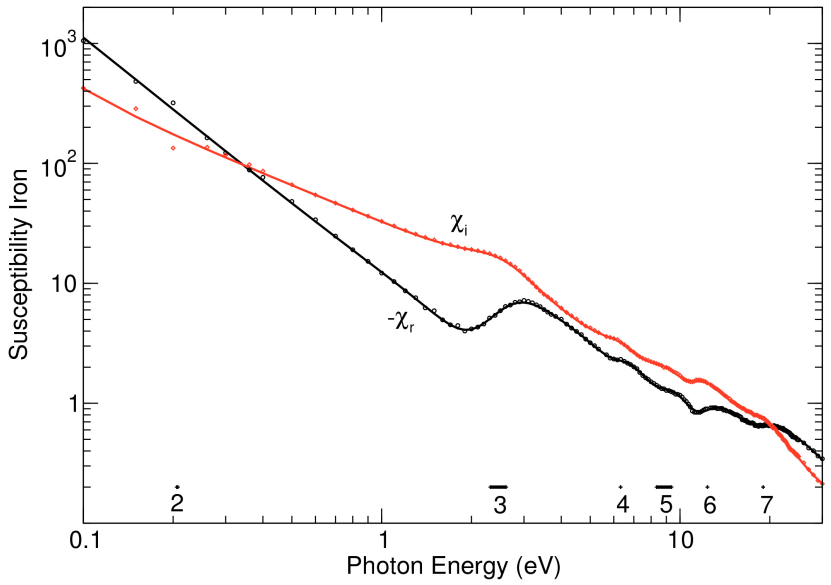

Figure 4. The real, χ_r, and imaginary, χ_i, parts of the susceptibility of iron using the BB model. Experimental values (small circles) were computed from the data in [19] [20]. The numbers above the abscissa represent the locations of transitions and the dashes above the numbers indicate the various values of σ_i, the degree of line broadening in the BB model.

values above the abscissa represent the transition energies and the dashes above the numbers indicate the broadening width. **Figure 4** shows that our improved BB model provides an accurate fit even for narrower inter-band transitions and validates that our model is applicable to iron up to 30 eV.

4. Conclusions

We analyzed the optical properties of Au, and Fe by using an improved Brendel-Bormann (BB) model. As an initial step, the Drude free electron theory is used to model the susceptibility of iron as illustrated in **Figure 2**. However, the differences between the Drude predictions and that of the experimental data are large, particularly in the near infrared region. The Drude-Lorentz extension places damped harmonic oscillators at critical points, referred to as inter-band transition points. In addition to the idea of the placement of oscillators at critical points, a Voigt lineshape assists in more accurately predicting susceptibility. Rakic *et al.* [17] used the BB method for various metals to show its accuracy for modeling the optical constants not only for amorphous solids but also for metals. We modified Rakic's model by reducing the number of unknowns, and relaxing a constraint from the system. **Table 2** shows that the largest concentrations of oscillators occur at $\omega_2 \approx 0.2\,\text{eV}$ and $\omega_7 \approx 20\,\text{eV}$. The large concentration at ω_2, about 32%, brings the imaginary part of the susceptibility, $-\chi_i$ in line with the experimental data, while the concentration at ω_7 tends to render the susceptibility to almost straight lines on the log-log plot in **Figure 4**. The fit of our model to iron data can be seen in **Figure 4**. The iron plot results up to 30 eV indicates that our model could perform fairly well for transition metals up to a broad range of the spectrum.

The studies that have been mentioned so far are related to diagonal elements of the relative permittivity tensor. However, one needs to take into account the off-diagonal elements if there is an external magnetic field in the anisotropic medium if the material is ferromagnetic. The off-diagonal elements were also incorporated by the contribution of Magneto-Optic Kerr Effect which includes the Kerr rotation angle and ellipticity [30]. The investigation of the off-diagonal elements was conducted by Krinchik *et al.* [31] [32] [33] by introducing the equatorial Kerr effect (T-MOKE) to the experimental setup.

Conflicts of Interest

The authors declare no conflicts of interest regarding the publication of this paper.

References

[1] Hammer, J.M., Evans, G.A., Özgür, G. and Butler, J.K. (2004) Isolators, Polarizers and Other Optical-Waveguide Devices Using a Resonant-Loss-Layer Effect. *Journal of Lightwave Technology*, **22**, 1754-1763. https://doi.org/10.1109/JLT.2004.831088

[2] Hammer, J.M., Evans, G.A., Özgür, G. and Butler, J.K. (2006) Integratable 40dB Optical Waveguide Isolators Using a Resonant Layer Effect with Mode Coupling. *Journal of Applied Physics*, **100**, Article ID: 103103. https://doi.org/10.1063/1.2388040

[3] Takenaka, M. and Nakano, Y. (1999) Proposal of a Novel Semiconductor Optical Waveguide Isolator. 11th *International Conference on Indium Phosphide and Related Materials*, Davos, 16-20 May 1999, 289-292.

[4] Yokoi, H., Mizumoto, T., Shinjo, N., Futakuchi, N. and Nakano, Y. (2000) Demonstration of an Optical Isolator with a Semiconductor Guiding Layer That Was Obtained by Use of a Nonreciprocal Phase Shift. *Applied Optics*, **39**, 6158-6164. https://doi.org/10.1364/AO.39.006158

[5] Zayet, W. and Ando, K. (1999) Optical Waveguide Isolator Based on Nonreciprocal Loss/Gain of Amplifier Covered by Ferromagnetic Layer. *IEEE Photonics Technology Letters*, **11**, 1012-1014. https://doi.org/10.1109/68.775330

[6] Ehrenreich, H. and Philipp, H.R. (1962) Optical Properties of Ag and Cu. *Physical Review*, **128**, 1622-1629. https://doi.org/10.1103/PhysRev.128.1622

[7] Adachi, S. (1987) Model Dielectric Constants of GaP, GaAs, GaSb, InP, InAs, and InSb. *Physical Review B*, **35**, 7454-7463. https://doi.org/10.1103/PhysRevB.35.7454

[8] Garland, J.W., Abad, H., Viccaro, M. and Raccah, P.M. (1988) Line Shape of the Optical Dielectric Function. *Applied Physics Letters*, **52**, 1176-1178. https://doi.org/10.1063/1.99641

[9] Oppeneer, P.M., Maurer, T., Sticht, J. and Kübler, J. (1992) *Ab Initio* Calculated Magneto-Optical Kerr Effect of Ferromagnetic Metals: Fe and Ni. *Physical Review B*, **45**, 10924-19933. https://doi.org/10.1103/PhysRevB.45.10924

[10] Brendel, R. and Bormann, D. (1992) An Infrared Dielectric Function Model for Amorphous Solids. *Journal of Applied Physics*, **71**, 1-6. https://doi.org/10.1063/1.350737

[11] Kim, C.C., Garland, J.W., Abad, H. and Raccah, P.M. (1992) Modeling the Optical Dielectric Function of Semiconductors: Extension of the Critical-Point Parabolic-Band Approximation. *Physical Review B*, **45**, 11749-11767. https://doi.org/10.1103/PhysRevB.45.11749

[12] Bennett, H.E. and Bennett, J.M. (1966) Validity of the Drude Theory for Silver, Gold and Aluminum in the Infrared. In: Abeles, F., Ed., *Optical Properties and Electronic Structure of Metals and Alloys*, North-Holland, Amsterdam, 175-186.

[13] Ordal, M.A., Long, L.L., Bell, R.J., S. Bell, E., Bell, R.R., Alexander Jr., R.W. and Ward, C.A. (1982) Optical Properties of the Metals Al, Co, Cu, Au, Fe, Pb, Ni, Pd, Pt, Ag, Ti, and W in the Infrared and Far Infrared. *Applied Optics*, **22**, 1099-1199. https://doi.org/10.1364/AO.22.001099

[14] Ordal, M.A., Bell, R.J., Alexander Jr., R.W., Long, L.L. and Querry, M.R. (1985) Optical Properties of Fourteen Metals in the Infrared and Far Infrared: Al, Co, Cu, Au, Fe, Pb, Mo, Ni, Pd, Pt, Ag, Ti, V, and W. *Applied Optics*, **24**, 4493-4499. https://doi.org/10.1364/AO.24.004493

[15] Powell, C.J. (1970) Analysis of Optical- and Inelastic-Electron-Scattering Data. II. Application to Al. *Journal of the Optical Society of America*, **60**, 78-93. https://doi.org/10.1364/JOSA.60.000078

[16] Rakić, A.D. (1995) Algorithm for the Determination of Intrinsic Optical Constants of Metal Films: Application to Aluminum. *Applied Optics*, **34**, 4755-4767. https://doi.org/10.1364/AO.34.004755

[17] Rakić, A.D., Djurisic, A.B., Elazar, J.M. and Majewski, M.L. (1998) Optical Properties of Metallic Films for Vertical-Cavity Optoelectronic Devices. *Applied Optics*, **37**, 5271-5283. https://doi.org/10.1364/AO.37.005271

[18] Djurisic, A.B. and Herbert Li, E. (1998) Modeling the Index of Refraction of Insulating Solids with a Modified Lorentz Oscillator Model. *Applied Optics*, **37**, 5291-5297. https://doi.org/10.1364/AO.37.005291

[19] Weaver, J.H., Krafka, C., Lynch, D.W. and Koch, E.E. (1981) Optical Properties of Metals. *Applied Optics*, **20**, 1124-1125. https://doi.org/10.1364/AO.20.1124_1

[20] Weaver, J. H., Krafka, C., Lynch, D.W. and Koch, E.E. (1981) Transition Metals. In *Optical Properties of Metals*, Zentralstelle fur Atomkernenergie-Dokumentation, Karlsruhe, Germany, 344 p.

[21] Kittel, C. (1996) Introduction to Solid State Physics. 7th Edition, John Wiley & Sons, Inc., New York.

[22] Johnson, P.B. and Christy, R.W. (1974) Optical Constants of Transition Metals: Ti, V, Cr, Mn, Fe, Co, Ni, and Pd. *Physical Review B*, **9**, 5056-5070. https://doi.org/10.1103/PhysRevB.9.5056

[23] Drude, P. (1900) Zur elektronentheorie der metalle. *Annalen der Physik*, **306**, 566-613. https://doi.org/10.1002/andp.19003060312

[24] Drude, P. (1902) The Theory of Optics. Longmans, Green, and Co., New York.

[25] Jackson, J.D. (1999) Classical Electrodynamics. 3rd Edition, John Wiley & Sons, Inc., New York.

[26] De, A. and Puri, A. (2002) Application of Plasma Resonance Condition for Prediction of Large Kerr Effects. *Journal of Applied Physics*, **92**, 5401-5408. https://doi.org/10.1063/1.1507816

[27] Is, H. (2010) Light Propagation in Waveguides Containing Ferromagnetic Layer. Master's Thesis, Southern Methodist University, Dallas.

[28] Mark 23 Library (2012) Optimization Section. https://www.nag.com/doc/inun/fs23/l6idcl/un.html

[29] Lynch, D.W., Hunter, W.R. and Palik, E.D. (1985) Handbook of Optical Constants of Solids. Vol. 1, Academic Press, Orlando.

[30] Oppeneer, H. (2001) Magneto-Optical Kerr Spectra. In: Buschow, K.H.J., Ed., *Handbook of Magnetic Materials*, Vol. 13, North Holland, Amsterdam, 234-236.

[31] Krinchik, G.S. and Nurmukhamedov, G.M. (1965) Experimental Investigation of the Electron Structure of Nickel by the Magneto-Optical Method. *Soviet Journal of Experimental and Theoretical Physics*, **21**, 22.

[32] Krinchik, G.S. (1957) Magneto-Optical Resonance in Ferromagnetics. *Vestnik Moskovskogo Universiteta. Seriya 1. Matematika. Mekhanika*, **12**, 87-98.

[33] Krinchik, G.S. and Artemjev, V.A. (1968) Magneto-Optic Properties of Nickel, Iron, and Cobalt. *Journal of Applied Physics*, **39**, 1276-1278. https://doi.org/10.1063/1.1656263

[34] Abramowitz, M. and Stegun, I.A., Eds. (1972) Handbook of Mathematical Functions. 10th Edition, Dover Publications, Inc., New York.

Appendix

It is convenient to write the closed form integrals that appear in the BB model of the dielectric constant/susceptibility tensors as a function of error integrals. In particular the expected value of the susceptibility given in (30) requires calculation of the expected value of the random variable $1/\tilde{\Omega}_i$

$$\begin{aligned} I(a_i) &= \left\langle \frac{1}{a_i^2 - \bar{\Omega}_i^2} \right\rangle = \frac{1}{\sqrt{2\pi}\sigma_i} \int_{-\infty}^{\infty} \frac{\mathrm{e}^{-(\bar{\omega}_i - \omega_i)^2/2\sigma_i^2}}{a_i^2 - \bar{\Omega}_i^2} \mathrm{d}\bar{\omega}_i \\ &= \frac{1}{\sqrt{2\pi}S_i} \int_{-\infty}^{\infty} \frac{\mathrm{e}^{-(\bar{\Omega}_i - \Omega_i)^2/2S_i^2}}{a_i^2 - \bar{\Omega}_i^2} \mathrm{d}\bar{\Omega}_i, \end{aligned} \tag{32}$$

where $S_i = \sigma_i/\omega$ is the variance of the random variable $\bar{\Omega}_i$, $a_i^2 = 1 - j\Gamma_i$. As described in Ref. [17], $I(a_i)$ can be written as a sum of 2 integrals by partial fraction expansion

$$\frac{1}{a_i^2 - \bar{\Omega}_i^2} = \frac{1}{2a_i}\left(\frac{1}{a_i - \bar{\Omega}_i} + \frac{1}{a_i + \bar{\Omega}_i}\right).$$

As required by convergence of the integral in (32), $\Im\{a_i\}$ must be positive so that

$$a_i = \frac{1}{\sqrt{2}}\left(-\sqrt{\sqrt{1+\Gamma_i^2}+1} + j\sqrt{\sqrt{1+\Gamma_i^2}-1}\right),$$

i.e., a_i must lie in the 2nd quadrant of the complex plane as opposed to the 4th quadrant (Equation (8) in Reference [17] has a different value for the sign of a_j'). The resulting integral in (32) produces

$$I(a_i) = -j\sqrt{\frac{\pi}{2}}\frac{1}{2S_i a_i}\left[w(z_1) + w(z_2)\right], \tag{33}$$

where $w(z) = \mathrm{e}^{-z^2}\mathrm{erfc}(-jz)$ is computed from the NAG Library, using function S15DDF, $z_1 = (a_i - \Omega_i)/\sqrt{2}S_i$, and $z_2 = (a_i + \Omega_i)/\sqrt{2}S_i$. The expected value of the off-diagonal element χ_o as given by (30) requires calculation of the expected value of the random variable $1/\tilde{\Omega}_i^2$, written as

$$J(a_i) = \left\langle \frac{1}{\tilde{\Omega}_i^2} \right\rangle = -\frac{1}{2a_i}\frac{\mathrm{d}I(a_i)}{\mathrm{d}a_i} = -j\frac{\sqrt{\pi}}{8a_i^3 S_i^2}\left(\sqrt{2}S_i(w_1 + w_2) - a_i(w_1' + w_2')\right) \tag{34}$$

The error functions and their derivatives are $w_k = w(z_k)$ and $w_k' = j\sqrt{2}/\pi - 2z_k w_k$, while $k = 1, 2$, respectively [34]. The recursion relation $w_k^{(n+2)} + 2z_k w_k^{(n+1)} + 2(n+1)w_k^{(n)} = 0$ can be used for higher order derivatives.